

pubs.acs.org/Macromolecules Article

# Diffusion of Thin Nanorods in Polymer Melts

Jiuling Wang, Thomas C. O'Connor, Gary S. Grest, Yitong Zheng, Michael Rubinstein, and Ting Ge\*



Cite This: Macromolecules 2021, 54, 7051-7059



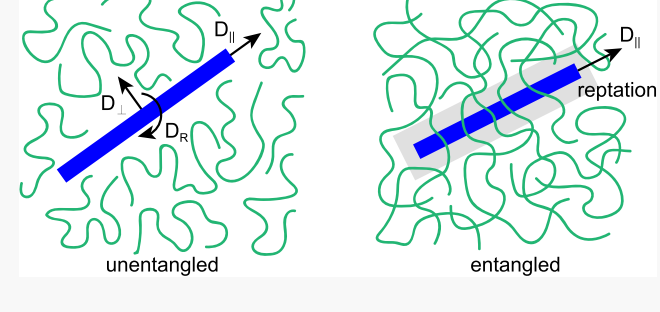
ACCESS

III Metrics & More



s Supporting Information

**ABSTRACT:** The diffusion of monomerically thin nanorods in polymer melts is studied by molecular dynamics simulations. We focus on the systems where the chains are long enough to screen the hydrodynamic interactions, in which case the diffusion coefficient  $D_{\parallel}$  for the direction parallel to the rod decreases linearly with increasing rod length l. In unentangled polymers, the diffusion coefficient for the direction normal to the rod exhibits a crossover from  $D_{\perp} \sim l^{-2}$  to  $\sim l^{-1}$  with increasing l, corresponding to a progressive coupling of nanorod motion to the polymers. Accordingly, the rotational diffusion coefficient  $D_{\rm R} \approx D_{\perp} l^{-2} \sim l^{-4}$  and then  $D_{\rm R} \sim l^{-3}$  as l increases. In entangled polymers,  $D_{\perp}$  and  $D_{\rm R}$ 



are suppressed for l larger than the entanglement mesh size a.  $D_{\perp} \sim l^{-3}$  and  $D_{R} \sim l^{-5}$  for l sufficiently above a, in agreement with de Gennes' rod reptation model.

#### 1. INTRODUCTION

Incorporation of nanorods into polymers can significantly improve the mechanical, 1-3 optical, 4-6 and electrical 7-11 properties of polymer matrices. While the spatial dispersion and organization of nanorods play critical roles in governing the properties of polymer—nanorod composites, 6,12-18 the dynamics of nanorods in polymers is not well understood, 19-21 which limits the ability to rationally manipulate the position and orientation of nanorods. Recent experiments also show that nanorods could be promising drug delivery carriers due to their superior transport capability in polymeric gels such as mucus; 22-26 however, the underlying mechanism is still elusive

While a continuum theory has been developed for a rodlike colloidal particle in a viscous fluid, <sup>27,28</sup> it cannot describe the diffusion of a nanorod in a polymer matrix. 20,21,29 A major reason is that the nanorod may not be fully coupled to the matrix, resulting in the breakdown of the continuum approximation. Such a breakdown has been established for spherical nanoparticles in a polymer matrix.<sup>30–37</sup> The friction coefficient for the diffusion of a spherical nanoparticle depends on the ratio of particle diameter to the chain size in unentangled polymer melts and the entanglement mesh size in entangled melts. Likewise, one would expect that the friction coefficient for the diffusion of nanorods in a polymer melt should also depend on the geometric parameters of the rod with respect to the length scales of the polymer. In recent experiments<sup>20</sup> and simulations,<sup>21</sup> it has already been shown that the diffusion coefficient of nanorods in polymer melts is higher than that predicted by the continuum theory.

One distinctive feature of the diffusion of a nanorod is the emergence of anisotropy in the translational diffusion parallel

and normal to the long axis of the rod. In addition to translational diffusion, a nanorod also undergoes rotational diffusion. The rotation couples the parallel and normal components of the translation in the body frame, and the overall translational diffusion is isotropic in the lab frame after the correlation of rod orientation with the initial orientation has decayed. Therefore, for nanorods, there are four distinct diffusion coefficients including the overall translational diffusion coefficient  $D_{\rm T}$ , the parallel component  $D_{\parallel}$ , the normal component  $D_{\perp}$ , and the rotational diffusion coefficient  $D_{\rm R}$ . Although the breakdown of the continuum description for nanorods in a polymer matrix has been observed in experiments 19,20 and simulations, 21 the rich features of the diffusion of nanorods in a polymer matrix have not been well studied

With the precise control of both nanorod geometry and polymer structure, molecular dynamics (MD) simulations can reveal how nanorod diffusion couples to a polymer matrix. Here, we present the results of extensive MD simulations of the diffusion of thin nanorods with a diameter equal to the monomer size in polymer melts in the dilute limit. Rod length l, polymer chain length N, and entanglement length  $N_{\rm e}$  are varied in the simulations. We characterize the scaling of various diffusion coefficients with l and how they are related to each other. We find that the diffusion coefficient of nanorods in

Received: May 5, 2021 Revised: June 17, 2021 Published: July 22, 2021





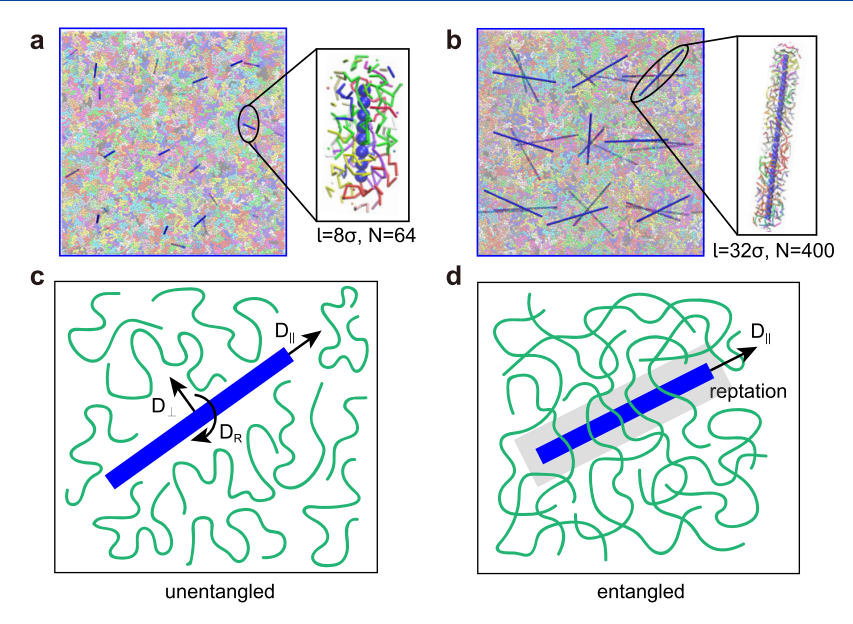


**Figure 1.** Snapshots of simulation samples of thin nanorods (blue) in polymer melts (mixed colors) for (a)  $l = 8\sigma$  in unentangled polymers of N = 64 and (b)  $l = 32\sigma$  in entangled polymers of N = 400. Schematic illustration of the diffusion of nanorods in (c) unentangled and (d) entangled polymer melts.

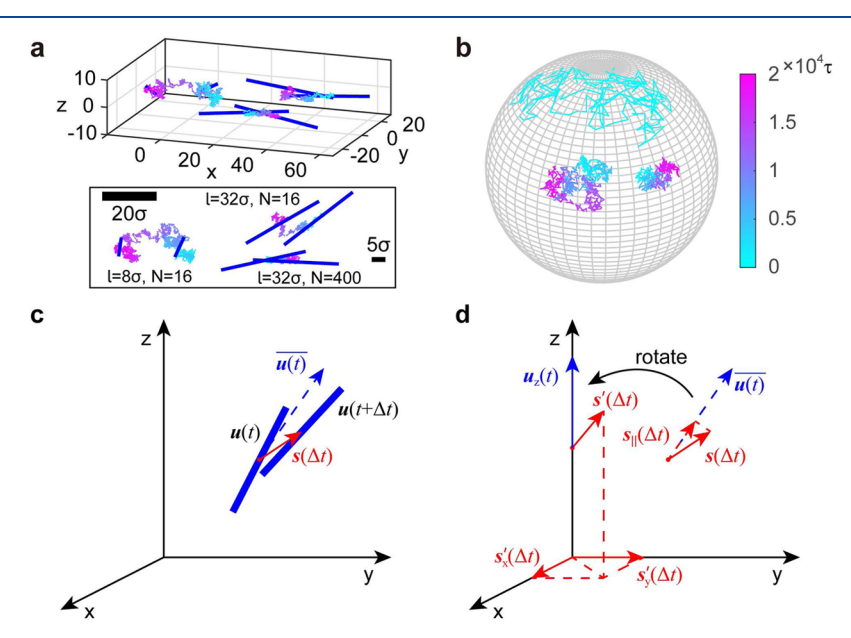


Figure 2. (a) Trajectories of thin nanorods in polymers (upper panel) and the projections to the xy plane (lower panel). The thick and thin bars in the lower panel indicate  $20\sigma$  and the entanglement mesh size  $5\sigma$ , respectively. (b) Rotational trajectories of the unit vector  $\mathbf{u}(t)$  along the rod axis for the same systems in (a). (c) Schematic illustration of orientational unit vectors  $\mathbf{u}(t)$  and  $\mathbf{u}(t+\Delta t)$  of the nanorod at time t and  $t+\Delta t$ .  $\overline{\mathbf{u}(t)}$  is the average of  $\mathbf{u}(t)$  and  $\mathbf{u}(t+\Delta t)$ , i.e.,  $\overline{\mathbf{u}(t)} = [\mathbf{u}(t) + \mathbf{u}(t+\Delta t)]/|\mathbf{u}(t) + \mathbf{u}(t+\Delta t)|$ . (d) Schematic illustration of the decomposition of the displacement  $\mathbf{s}(\Delta t)$  of a nanorod over a short time interval  $\Delta t$  to the parallel and normal components.

polymer melts does not scale with rod length l like that of spherical nanoparticles does with sphere diameter d. This unanticipated behavior reveals the role of particle shape in the coupling of nanoparticles to the polymer matrix.

### 2. MODELS AND METHODS

**2.1. Simulation Models.** The canonical bead-spring model of polymers  $^{39-41}$  is used in the simulations. Monomers of size  $\sigma$  and mass m interact via the Lennard-Jones (LJ) potential with an interaction strength  $\epsilon$ , cutoff distance  $r_{\rm c}=2.5\sigma$ , and characteristic time scale  $\tau=\sigma\sqrt{m/\epsilon}$ . Chains of N=2-2000 monomers are connected by finitely extensible nonlinear elastic (FENE) bonds. Chain stiffness

is varied by a bond bending potential  $V_{\theta} = k_{\theta}(1 + \cos \theta)$ , where  $\theta$  is the angle between two consecutive bonds. We modeled polymer chains with  $k_{\theta} = 0$ ,  $1.5\epsilon$  and  $3.0\epsilon$ , which gives Kuhn lengths  $l_{\rm K} = 1.9\sigma$ ,  $2.9\sigma$  and  $5.0\sigma$ , respectively. We also simulated rods in an LJ fluid (N = 1).

Nanorods are modeled as rigid bodies made of beads similar to the monomers. A nanorod of length l is made of  $l/\sigma$  beads of size  $\sigma$  and mass m that are placed along a straight line with regular spacing  $\sigma$ . Nanorod beads interact with polymer beads via a LJ potential with  $r_c = 2.5\sigma$ , which promotes the dispersion of nanorods in the melt. Meanwhile, the LJ interaction between beads on two nanorods is purely repulsive  $(r_c = 2^{1/6}\sigma)$  to prevent the aggregation of nanorods. To equilibrate the nanorods in polymer melts, each sample was

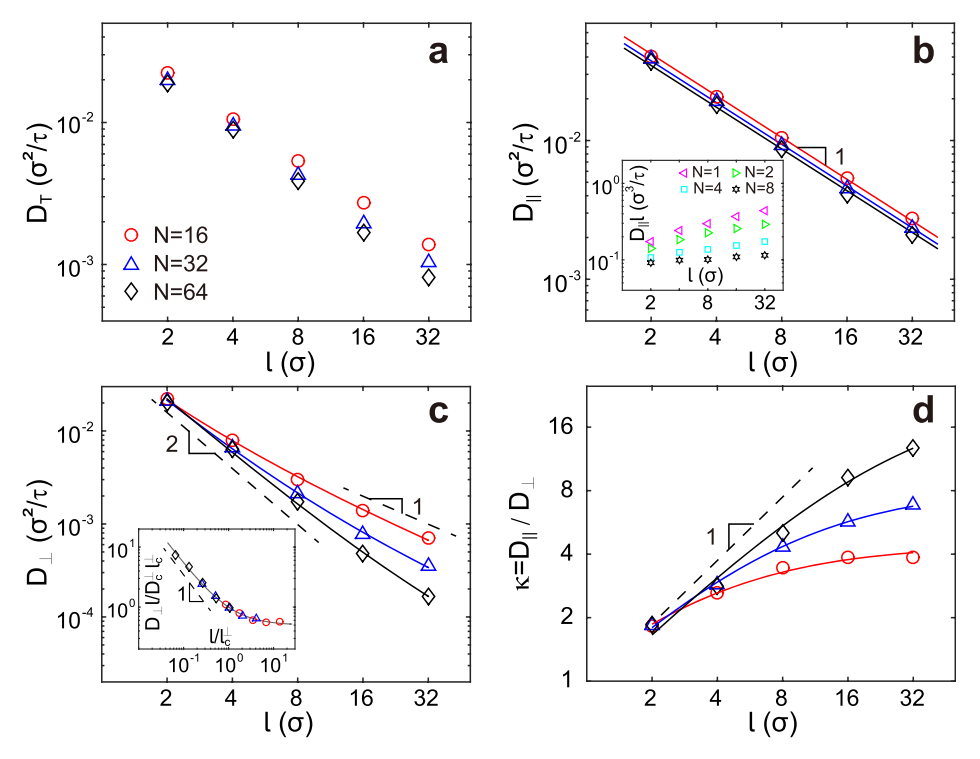


Figure 3. (a) Overall translational diffusion coefficient  $D_{\rm T}$ , (b) parallel component  $D_{\parallel}$  and the best fits to a linear function, (c) normal component  $D_{\perp}$  and the best fits to a crossover function from  $D_{\perp} \sim l^{-2}$  to  $\sim l^{-1}$ , and (d) diffusion anisotropy  $\kappa = D_{\parallel}/D_{\perp}$  and the best fits to a crossover function from  $\kappa \sim l$  to  $\kappa = 0$  and indicated  $\kappa = 0$ . The values of fitting parameters for the best-fit lines are presented in the SI. The inset of (b) shows  $D_{\parallel}l$  for the systems with N = 1, 2, 4, and 8. The inset of (c) shows the collapse of the rescaled simulation data for  $D_{\perp}$ .

simulated with a cubic box of side length L and periodic boundary conditions in all three directions. Two representative samples are visualized in Figure 1a,1b, respectively. All samples were equilibrated at temperature  $T = 1.0\epsilon/k_{\rm B}$  and pressure P = 0 except for N = 1, where  $P = 0.5\epsilon/\sigma^3$ . During the equilibration, a Nosé-Hoover thermostat/barostat was applied to the matrix chains, while a Nosé-Hoover thermostat was used to equilibrate both the translational and rotational degrees of freedom of the rigid nanorods. System parameters for the nanorods in polymer chains with stiffness  $k_{\theta} = 0$ , 1.5 $\epsilon$ , and 3.0 $\epsilon$  are listed in Tables S1-S3 in the Supporting Information (SI), respectively. The number of nanorods was  $N_r = 27$ in all samples except for N = 2000, where  $N_r = 50$ , while the number of matrix chains  $N_c$  was varied. The volume fraction of the nanorods  $\phi_r = N_r l d^2 / L^3$ , where d and l are the diameter and length of the nanorods, is between 0.004 and 0.07% in all samples. The excluded volume of a nanorod is  $v_{exl} = l^2 d$ , and the volume fraction of the excluded volumes of the nanorods  $\phi_{\rm exl} = N_{\rm r} v_{\rm exl} / L^3$  is less than 2.1% in all samples. The nanorods are well dispersed without any aggregation during our simulations. This is demonstrated by the steady large value of the radius of gyration  $R_g$  of the  $N_r$  nanorods over time (see Figure S1 of the SI). The model used here can be extended to further study the effects of nanorod diameter and interaction strength with polymers in the future.

Diffusion of nanorods in polymer melts at equilibrium was simulated at a fixed volume and a constant temperature  $T=1.0\epsilon/k_{\rm B}$ . The temperature of matrix chains was controlled using a Nosé–Hoover thermostat with a damping time of  $10\tau$ . The temperature for the translation and rotation of a rigid nanorod was maintained by a separate Nosé–Hoover thermostat with a damping time of  $10\tau$ . Depending on N and l, the simulations were run from  $8\times 10^4\tau$  to  $2\times 10^6\tau$  for  $k_{\theta}=0$ , from  $6\times 10^4\tau$  to  $1\times 10^7\tau$  for  $k_{\theta}=1.5\epsilon$ , and from  $6\times 10^4\tau$  to  $5\times 10^6\tau$  for  $k_{\theta}=3.0\epsilon$ . The time step was  $0.01\tau$ . All of the simulations were performed using the LAMMPS simulation package. 43

**2.2. Calculation of D\_T, D\_{\parallel}, and D\_{\perp}.** We computed the mean-square displacement (MSD)  $\langle \Delta r^2(t) \rangle = \langle [r_{\rm com}(t) - r_{\rm com}(0)]^2 \rangle$  of the

center of mass of nanorods as a function of time t in the polymer melts. The overall translational diffusion coefficient  $D_{\rm T}$  was extracted from the long-time limit of  $\langle \Delta r^2(t) \rangle/6t$ .  $\langle \Delta r^2(t) \rangle$  and  $\langle \Delta r^2(t) \rangle/6t$  for two sets of simulations are shown in Figures S2 and S3.

The translational diffusion can be decomposed to parallel and normal components, as schematically shown in Figure 1c. We decomposed the displacement of a nanorod to its parallel and normal components using a numerical procedure similar to that in ref 38. The procedure is illustrated in Figure 2c,d. The parallel component is the displacement of the center of mass of nanorods along the rod axis in the body frame, whereas the normal component is the displacement perpendicular to the axis. From t to  $t + \Delta t$  with a time interval  $\Delta t$ , the unit vector along the nanorod changes from u(t) to  $u(t + \Delta t)$ , as shown in Figure 2c. The center-of-mass displacement of the nanorod is  $s(\Delta t)$ , and the parallel component  $s_{\parallel}(\Delta t) = [s(\Delta t) \cdot u(t)]u(t)$ , where  $\overline{u(t)}$  is the average of u(t) and  $u(t + \Delta t)$ , as shown in Figure 2d. The displacement  $s_{\parallel}(t)$  along the nanorod axis over time t is obtained by summing the parallel displacements in successive time intervals, i.e.,  $s_{\parallel}(t) = \sum s_{\parallel}(\Delta t)$ . The parallel component of MSD  $\langle \Delta r_{\parallel}^2(t) \rangle =$  $\langle s_{\parallel}^2(t) \rangle$ . The diffusion coefficient  $D_{\parallel}$  along the rod axis is determined as the long-time limit of  $\langle \Delta r_{\parallel}^2(t) \rangle / 2t$ .

To obtain the normal component of nanorod displacement, we first rotate the unit vector  $\overline{u(t)}$  about an axis  $u_{axis}(t)$  so that  $\overline{u(t)}$  aligns with the z-axis  $u_z$  in the lab frame. The rotation axis is  $u_{axis}(t) = \overline{u(t)} \times u_z$ , and the rotation angle is  $\omega(t) = \cos^{-1}[\overline{u(t)} \cdot u_z]$ . Using the same axis  $u_{axis}(t)$  and angle  $\omega(t)$ , we then rotate the displacement vector  $s(\Delta t)$  to a new vector  $s'(\Delta t)$ . The projections of  $s'(\Delta t)$  to the x-axis and y-axis are  $s_x'(\Delta t)$  and  $s_y'(\Delta t)$ , as illustrated in Figure 2d. The body-frame displacement  $s_\perp(t)$  perpendicular to the nanorod axis is obtained by summing over  $s_x'(\Delta t)$  and  $s_y'(\Delta t)$  in successive time intervals, i.e.,  $s_\perp(t) = \sum [s_x'(\Delta t) + s_y'(\Delta t)]$ . The normal component of MSD  $\langle \Delta r_\perp^2(t) \rangle = \langle s_\perp^2(t) \rangle$ . The diffusion coefficient  $D_\perp$  perpendicular to the nanorod axis is determined as the long-time limit of  $\langle \Delta r_\perp^2(t) \rangle / 4t$ .

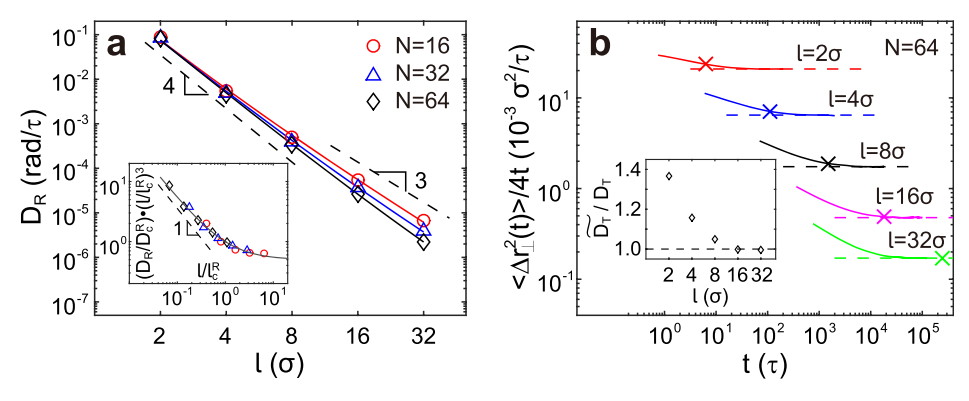


Figure 4. (a) Rotational diffusion coefficient  $D_R$  vs l for the nanorods in unentangled polymers of  $k_\theta=0$  and indicated N. Solid lines are best-fit lines to a crossover function from  $D_R \sim l^{-4}$  to  $\sim l^{-3}$ . The inset shows the collapse of the rescaled data for different N values. (b)  $\langle \Delta r_\perp^2(t) \rangle / 4t$ , where  $\langle \Delta r_\perp^2(t) \rangle$  is the mean-square displacement normal to the rod axis versus time for N=64. The rotational diffusion time  $\tau_R$  is marked on the line. The inset shows  $\widetilde{D_T}/D_T$  vs l, where  $\widetilde{D_T}=(D_\parallel+2D_\perp)/3$ .

The accuracy of the decomposition depends on the time interval  $\Delta t$ . The angle  $\Delta \theta = \cos^{-1}[u(t) \cdot u(t+\Delta t)]$  for the rotation of the nanorod during the time interval  $\Delta t$  needs to be small enough. Figures S4 and S5 show the results of decomposition converge for  $\Delta \theta < 10^\circ$ . For all results presented, we ensured that  $\Delta \theta < 10^\circ$ . The decompositions of the overall displacements in Figures S2 and S3 are shown in Figures S6 and S7, respectively.

**2.3. Calculation of**  $D_R$ . The rational diffusion of a nanorod is schematically shown in Figure 1c. To characterize the rotational diffusion, we followed the unit vector u(t) along the nanorod axis as a function of time t. Three representative rotational trajectories of u(t) are shown in Figure 2b. The rotational diffusion coefficient  $D_R$  is calculated based on the mean-square angular displacement (MSAD) of nanorods, MSAD =  $\langle |u(t) - u(0)|^2 \rangle$ . In the large-time limit, MSAD =  $2[1 - \exp(-2D_R t)]$ . MSAD curves for the two sets of simulations in Figures S2 and S3 are shown in Figures S8 and S9.

Although the nanorods are well dispersed and well separated from each other in our simulations, the long-range hydrodynamic effect may affect the diffusion coefficients of nanorods. For a single spherical nanoparticle that is larger than the fluid molecules, the translational diffusion coefficient  $D_{\rm T}(L)$  in a finite simulation box of size L is affected by the long-range hydrodynamics, and a term  $-2.837k_{\rm B}T/6\pi\eta L$ , where  $\eta$  is the bulk viscosity of the fluid, has been used to correct the long-range hydrodynamic effect. <sup>44–46</sup> For multiple rodlike nanoparticles in the present simulations, no numerical expressions correcting the long-range hydrodynamic effect exist. A systematic study to determine the correction terms for various diffusion coefficients of the nanorods with different rod lengths in different chain lengths requires extensive computational resources and is beyond the scope of the current study.

## 3. RESULTS AND DISCUSSION

3.1. Diffusion of Nanorods in Unentangled Polymer Melts. We first consider nanorod diffusion in three unentangled melts with N = 16, 32, and 64, all of which are below the entanglement length  $N_{\rm e}$  = 85 for  $k_{\theta}$  = 0. Results for the translational diffusion of nanorods are presented in Figure 3. Simulations allow us to separately obtain  $D_T$ ,  $D_{\parallel}$ , and  $D_{\perp}$ from their respective mean-square displacements (MSDs) as functions of time (see Section S2 in the SI for the MSDs). All three diffusion coefficients in Figure 3a-c generally decrease with increasing *l* as nanorods experience more drag from the surrounding polymers.  $D_{\parallel}$  decreases linearly with increasing lin melts of N = 16, 32, and 64. Solid lines in Figure 3b show the best fits to  $D_{\parallel} = D_0 (l/\sigma)^{-1}$ , where  $D_0$  is the monomeric diffusion coefficient for  $l/\sigma = 1$ . According to the Einstein relation, the parallel friction coefficient  $\zeta_{\parallel} = k_{\rm B} T/D_{\parallel}$  increases linearly with l. Each of the  $l/\sigma$  beads couples to a local region of monomer size and experiences a monomeric friction  $\zeta_0^l$ . This gives rise to  $\zeta_{\parallel} = \zeta_0^{\parallel}(l/\sigma)$ .  $^{47}$  Each individual  $\zeta_0^{\parallel}$  contributes independently to  $\zeta_{\parallel}$  as the hydrodynamic interactions between different beads are screened. In contrast, the hydrodynamic interactions are not screened in the melts of shorter chains with N=2, 4, and 8 and in the LJ fluid (N=1). As shown in the inset of Figure 3b,  $D_{\parallel}$  l increases with l rather than being constant for  $N \leq 8$ , indicating that the unscreened hydrodynamic interactions reduce the friction with respect to  $\zeta_{\parallel} = \zeta_0^{\parallel}(l/\sigma)$ . The focus of this paper is the systems of  $N \geq 16$ .

The cross section of the nanorod depends upon the direction of its motion, which produces qualitative differences in the diffusion normal and parallel to the rod axis.  $D_{\perp}$  is significantly smaller than  $D_{\parallel}$  and initially decreases unexpectedly as  $D_{\perp} \sim l^{-2}$  before crossing over to  $D_{\perp} \sim l^{-1}$  as l increases. As shown in Figure 3c,  $D_{\perp}$  for  $N \ge 16$  can be fitted with function  $D_{\perp} = D_{\rm c}^{\perp} [1 + (l/l_{\rm c}^{\perp})]/[2(l/l_{\rm c}^{\perp})^2]$ , where  $D_{\rm c}^{\perp}$  is the diffusion coefficient at the crossover rod length  $l_c^{\perp}$ . A good collapse of the simulation data rescaled by the best-fit values of  $D_c^{\perp}$  and  $l_c^{\perp}$  is shown in the inset of Figure 3c. The first regime  $D_{\perp} \sim l^{-2}$  indicates a progressive coupling of nanorods to longer chain segments and eventually the entire polymer chains as l increases. This can be seen by noting that  $D_{\perp} \sim l^{-2}$  implies that the perpendicular friction per unit length  $\zeta_{\perp}/l \sim D_{\perp}^{-1}l^{-1}$  grows linearly with increasing l. The second regime  $D_{\perp} \sim l^{-1}$ indicates saturation of the perpendicular friction per unit length for sufficiently large l.

We can compare the diffusion normal to the rod axis and that of a spherical nanoparticle in the same unentangled polymer melts. Scaling theories<sup>31,48</sup> show that the friction coefficient of a spherical particle increases from the monomeric friction  $\zeta_0$  for d comparable to the monomer size b as  $\zeta \approx$  $\zeta_0(d/b)^3$  until d is comparable to the melt chain size R. As d exceeds R,  $\zeta$  is given by Stokes' law,  $\zeta = f\eta_{\text{melt}}d$ , where f is a numerical prefactor and  $\eta_{\rm melt}$  is the bulk melt viscosity. Our simulations reveal  $\zeta_{\perp} \sim l^2$  for a nanorod in the first regime. This differs from  $\zeta \sim l^3$  of a sphere with similar  $d \approx l < R$ , indicating that the shape plays a role in the dynamical coupling of anisotropic nanoparticles and polymer melts, which needs to be included in a theoretical description. <sup>49</sup>  $\zeta_{\perp} \sim l$  of a nanorod in the second regime is reminiscent of  $\zeta \sim l$  of a sphere with d $\approx l > R$ . Previous theory for rodlike colloidal particles of length  $\overline{l}$  and diameter  $\overline{d}$  in a viscous fluid of viscosity  $\eta_s$  shows that  $\zeta_\perp$  $\approx \eta_s \overline{l}/\ln(\overline{l}/\overline{d})$  with the logarithmic term correcting for the unscreened hydrodynamic interactions among different

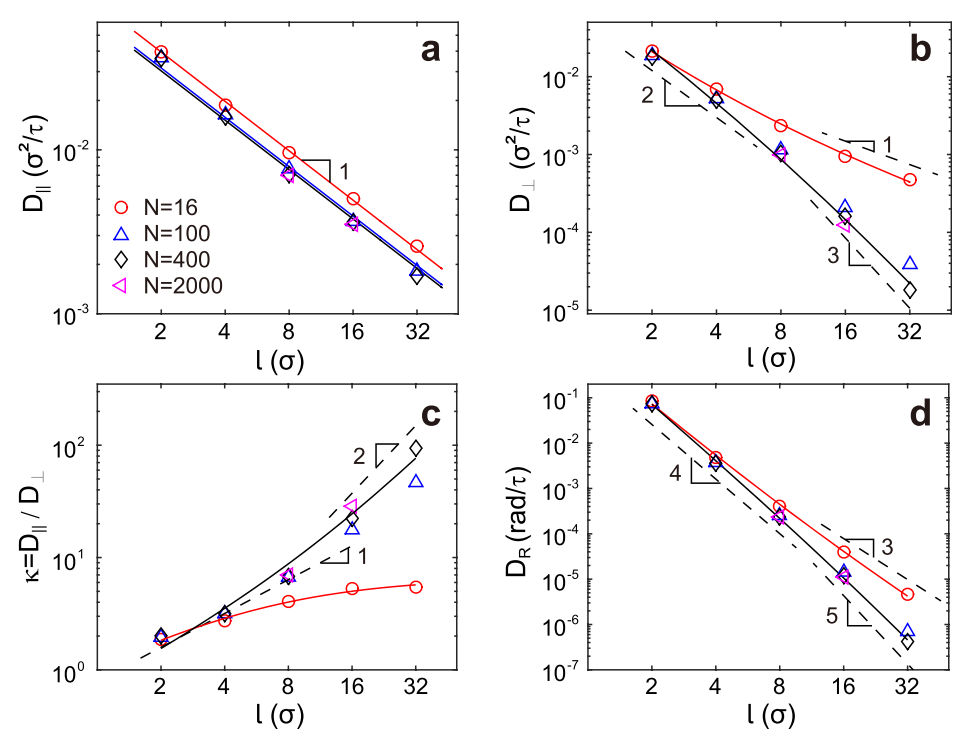


Figure 5. (a)  $D_{\parallel}$ , (b)  $D_{\perp}$ , and (c)  $\kappa = D_{\parallel}/D_{\perp}$  for the translational diffusion and (d)  $D_{\rm R}$  for the rotational diffusion of nanorods in polymer melts of N=16, 100, 400, and 2000 with  $k_{\theta}=1.5\epsilon$ . Solid lines indicate the best fits to the crossover functions, while dashed lines indicate the scaling exponents. Best-fit values of the fitting parameters are presented in the SI.

sections of the rod.<sup>27</sup> There is currently no theory relating  $\zeta_{\perp}$  to  $\eta_{\rm melt}$  for a nanorod in a polymer melt with the hydrodynamic interactions "partially" screened as in the simulations of  $N \geq 16$ . Numerically,  $\zeta_{\perp} = (2.7 \pm 0.1) \eta_{\rm melt} l$  for  $l = 32\sigma$  in the melts of N = 16 with  $k_{\theta}/\epsilon = 0$ , 1.5, and 3 (see Section S4 in the SI for the values of  $\eta_{\rm melt}$ ).

The total translational diffusion  $D_{\rm T}$  is dominated by the motion along the rod axis as l increases. The diffusion anisotropy  $\kappa = D_{\parallel}/D_{\perp}$  is shown in Figure 3d.  $\kappa$  first increases linearly with l because  $\kappa = \zeta_{\perp}/\zeta_{\parallel} \sim l^2/l \sim l$ . For N=16,  $\kappa$  eventually levels off as both  $D_{\parallel}$  and  $D_{\perp}$  scale as  $l^{-1}$  for sufficiently large 1. For N=32 and 64,  $\kappa$  has not completely leveled off, as  $D_{\perp} \sim l^{-1}$  has not fully developed at  $l = 32\sigma$ . Solid lines in Figure 3d are the best fits to  $\kappa = 2\kappa_c(l/l_c^{\kappa})/[1 + (l/l_c^{\kappa})]$ , where  $\kappa_c$  is the diffusion anisotropy at the crossover rod length  $l_c^{\kappa}$ . The fundamental reason for the diffusion anisotropy is that while the parallel component is coupled only to surrounding monomers, the normal component is progressively coupled to larger chain segments and eventually entire polymer chains with increasing  $l. \kappa = 2$  in the continuum theory for rodlike colloidal particles as both parallel and perpendicular components of the diffusion experience the same viscosity  $\eta_s$ .  $\kappa$  at saturation for monomerically thin nanorods in an unentangled polymer melt can be much larger than 2 and is controlled by  $\eta_{\mathrm{mel} v}$  which determines  $\zeta_{\perp}$  as  $\kappa$  saturates.

Nanorods also undergo rotational diffusion that couples the parallel and perpendicular components of the translational diffusion in their body frame. Understanding how this coupling is related to nanoparticle shape is essential for extracting accurate diffusion data from micro- and nanorheology experiments. Results for  $D_{\rm R}$  of the rods in unentangled melts are shown in Figure 4a.  $D_{\rm R}$  shows a strong decrease with increasing l. This is illustrated in Figure 2b, which shows the rotational trajectories swept by several rods of different l over

the same time period. In all systems, the decrease of  $D_{\rm R}$  exhibits a crossover from  $D_{\rm R}\sim l^{-4}$  to  $\sim l^{-3}$ , which can be fit by a crossover function  $D_{\rm R}=D_{\rm c}^{\rm R}[1+(l/l_{\rm c}^{\rm R})]/[2(l/l_{\rm c}^{\rm R})^4]$ , where  $D_{\rm c}^{\rm R}$  is the diffusion coefficient at the crossover rod length  $l_{\rm c}^{\rm R}$ . The inset of Figure 4a shows that the simulation data collapse when rescaled by the best-fit values of  $D_{\rm c}^{\rm R}$  and  $l_{\rm c}^{\rm R}$  for different N values. The scaling behavior observed for  $D_{\rm R}$  is related to that of  $D_{\perp}$  as  $D_{\rm R}\approx D_{\perp}l^{-2}$ . Therefore, the crossover from  $D_{\rm R}\sim l^{-4}$  to  $\sim l^{-3}$  corresponds to the crossover from  $D_{\perp}\sim l^{-2}$  to  $\sim l^{-1}$  and is a consequence of the progressive coupling to the polymer matrix.

The crossover rod lengths  $l_c^{\perp}$ ,  $l_c^{\kappa}$  and  $l_c^{R}$  all correspond to the rod length above which the nanorods are coupled to the entire polymer chains. As a result, one would expect they are controlled by the polymer chain size. We compare  $l_c^{\perp}$ ,  $l_c^{\kappa}$ ,  $l_c^{R}$  and the root mean squared end-to-end size  $R_{\rm ee}$  of polymer chains for N=16, 32, and 64 in Figure S10 of the SI. The crossover rod lengths and average polymer size all increase with N, but they are not related by constant numerical factors. What determines the crossover rod lengths is an open question that needs further study.

The rotational diffusion time  $\tau_{\rm R}=1/2D_{\rm R}$  for the nanorods in chains of N=64 are indicated by cross symbols on the lines of  $\langle \Delta r_{\perp}^2(t) \rangle/4t$  in Figure 4b, where  $\langle \Delta r_{\perp}^2(t) \rangle$  is the MSD of nanorods normal to the rod axis in the body frame. The plateau of  $\langle \Delta r_{\perp}^2(t) \rangle/4t$  indicates the diffusive regime, with the onset of the plateau corresponding to the translational diffusion time  $\tau_{\rm T}$  in the body frame. The plateau. As a result, rotation of the rod accompanies each diffusion time step in the body frame and couples the orthogonal components.  $D_{\rm T}=(D_{\parallel}+2D_{\perp})/3$  based on independent  $D_{\parallel}$  and  $D_{\perp}$  overpredicts  $D_{\rm T}$  in the lab frame, as shown in the inset of Figure 4b. For  $l \geq 16\sigma$ ,  $\tau_{\rm R}$  is on the plateau. There is no significant rotation for each diffusion time

step in the body frame. Therefore, the body and lab frames are equivalent at the diffusion time scale  $\tau_{\rm T}$ , and  $D_{\rm T} = \widetilde{D_{\rm T}}$  is valid for  $l \geq 16\sigma$ .

**3.2.** Diffusion of Nanorods in Entangled Polymer Melts. As the polymer chain length N increases above the entanglement length  $N_{\rm e}$ , the polymer entanglement network affects diffusion of the nanorods longer than the network mesh size a. Figure 5 shows  $D_{\parallel}$ ,  $D_{\perp}$ ,  $\kappa$ , and  $D_{\rm R}$  as functions of l for nanorods in polymer melts with  $k_{\theta}=1.5\epsilon$ . The entanglement length is reduced to  $N_{\rm e}=28$  for  $k_{\theta}=1.5\epsilon$ . Note that  $k_{\theta}=0$  and  $N_{\rm e}=85$  for the simulations of unentangled systems in Section 3.1. The polymer melts with N=16, 100, 400, and 2000 in this section correspond to  $Z=N/N_{\rm e}=0.6$ , 3.6, 14, and 71, respectively.

The linear decrease of  $D_{\parallel}$  with l is not affected by the presence of an entanglement network since the diameter of the rod  $\sigma$  is smaller than the network mesh size  $a \approx 5\sigma$ . Solid lines in Figure 5a are best fits to  $D_{\parallel} = D_0 (l/\sigma)^{-1}$ . In contrast,  $D_{\perp}$  is suppressed as l grows larger than a. Figure 5b shows that  $D_{\perp} \sim$  $l^{-2}$  for  $l \leq 8\sigma$  in entangled chains with  $N \geq 100$   $(Z \geq 4)$  is unchanged from the first scaling regime  $D_{\perp} \sim l^{-2}$  in unentangled chains. While there is a crossover to  $D_{\perp} \sim l^{-1}$ in the unentangled melt of N = 16 (see the red solid line in Figure 5b), the entangled systems exhibit a steeper decrease in  $D_{\perp}$  for  $l \geq 16\sigma$ . Figure 2a illustrates the suppression of perpendicular diffusion for the rods of  $l = 32\sigma$  in the entangled melt of N = 400. To describe the motion of a nanorod trapped in an entanglement network, de Gennes developed a rod "reptation" model,<sup>53</sup> as schematically illustrated in Figure 1d. In  $\hat{h}$ is model, as the rod reptates over a distance of its length lwith  $D_{\rm T} \approx D_{\parallel}$ , the displacement due to normal diffusion  $\approx a$ . From  $l^2/D_{\parallel} \approx a^2/D_{\perp}$ ,  $D_{\perp} \approx D_{\parallel}(a/l)^2 \sim l^{-3}$ . As shown by the black solid line in Figure 5b,  $D_{\perp}$  for N = 400 can be fit to the crossover function  $D_{\perp} = 2D_c^{\perp}/[(l/l_c^{\perp})^2 + (l/l_c^{\perp})^3]$ , indicating that  $D_{\perp} \sim l^{-3}$  for l sufficiently larger than a in agreement with de Gennes' reptation model. Figure 5c shows the suppression of  $D_{\perp}$  enhances  $\kappa$ , which no longer plateaus as in unentangled polymers (red solid line), but instead grows as  $l^2$  for large l. The black solid line in Figure 5c is the best fit of  $\kappa$  for N = 400to the crossover function  $\kappa = \kappa_c [(l/l_c^{\kappa}) + (l/l_c^{\kappa})^2]/2$ .  $\kappa \sim l^2$  as  $D_{\perp}$ is reduced by a factor  $\approx (l/a)^2$  compared to  $D_{\parallel}$ . This large ratio means the diffusion of nanorods is dominated by the motion parallel to the rod axis, which only depends on the local dynamics of polymer segments. This result agrees with the experimental observation by Choi et al. that the dynamics of nanorods is decoupled from the macroscopic viscosity of polymer melts and thus is only coupled to the local dynamics.<sup>20</sup> As the rod diameter goes above a, one would expect suppression of the parallel diffusion as well. The diffusion of the fat nanorod would rely on the relaxation of the surrounding entanglement network as in the diffusion of a spherical particle with d > a in an entangled polymer melt.  $^{32,54,55}$ 

The rotational diffusion also exhibits a suppression as l is sufficiently larger than a. Rather than crossing over from  $D_{\rm R} \sim l^{-4}$  to  $\sim l^{-3}$ ,  $D_{\rm R}$  in entangled polymers transitions to  $D_{\rm R} \approx D_{\perp} l^{-2} \sim l^{-5}$ .  $D_{\rm R}$  for N=400 in Figure 5d can be fit to the crossover function  $D_{\rm R}=2D_{\rm c}^{\rm R}/[(l/l_{\rm c}^{\rm R})^4+(l/l_{\rm c}^{\rm R})^5]$ . The suppression clearly distinguishes the rotational trajectory of a rod of  $l=32\sigma$  in the chains of N=400, as shown in Figure 2b.

chains of N=400, as shown in Figure 2b.

The crossover rod lengths  $l_c^L$ ,  $l_c^R$  for N=400 in Figure 5 all correspond to the rod length above which nanorods are affected by the entanglement network. The crossover rod

lengths are expected to be controlled by the network mesh size. As shown in Section 3.2 of the SI,  $l_c^{\perp}/a = 1.7$ ,  $l_c^{\kappa}/a = 2.5$ , and  $l_c^{R}/a = 3.9$ , suggesting that the rod length needs to be multiple a for the suppression of nanorod motion.

Using MD simulations, Karatrantos et al.21 have shown that thin nanorods in polymer melts can diffuse faster than predicted by the continuum theory and the diffusion coefficient reaches a plateau as melt chain length N increases, both of which were attributed to local viscosity experienced by nanorods. The N-dependency of the diffusion of thin nanorods in polymer melts has also been examined in the simulations by Li et al. 29 The N-dependent translational diffusion in unentangled melts and N-independent translational diffusion in entangled melts in their simulations were related to the difference between the diffusion parallel and perpendicular to the rod axis. In this work, by decomposing the diffusion into parallel and perpendicular components, we explicitly show thin nanorods only experience monomeric friction for the diffusion parallel to the rod axis and the parallel component  $D_{\parallel}$ dominates the overall diffusivity, which is the origin of the breakdown of the continuum theory. These findings are consistent with previous simulations. Furthermore, by identifying the scaling of various diffusion coefficients  $D_{\parallel}$ ,  $D_{\perp}$ , and  $D_R$  with rod length l, we elucidate the length-scaledependent coupling of nanorod dynamics to the polymer

For spherical nanoparticles in polymer melts, the dynamical coupling between the nanoparticles and polymers has been described through extending the Stokes-Einstein relation  $D_{\rm SE}$ =  $k_{\rm B}T/\zeta = k_{\rm B}T/3\pi\eta d$  for a particle of diameter d in a medium of viscosity  $\eta$ . The essential part of the extension involves a replacement of the bulk viscosity  $\eta$  by an effective viscosity  $\eta_{\rm eff}$ that depends on the nanoparticle diameter d. 31,54,55 Since the bulk viscosity is related to the stress relaxation modulus G(t) of polymer dynamics as  $\eta = \int_0^\infty G(t) dt$ ,  $\eta_{\text{eff}} < \eta$  corresponds to coupling to only part of the polymer dynamics, which can be quantified by an effective relaxation modulus  $G_{\text{eff}}(t)$ .  $\eta_{\text{eff}}$  =  $\int_0^\infty G_{\text{eff}}(t) dt$ , and  $G_{\text{eff}}(t)$  for the partial coupling can be obtained from the MSD of nanopartiles by the generalized Stokes–Einstein relation. 35,56–59 For rodlike nanoparticles in polymer melts, the dynamical coupling of nanoparticles and polymers may also be quantitatively described by invoking an effective viscosity  $\eta_{\rm eff}$  and an effective relaxation modulus  $G_{\rm eff}(t)$ . Specifically,  $\eta_{\rm eff}$  may be introduced as in a recent scaling model of the dynamical coupling in liquid polyelectrolyte coacervates,  $^{60}$  and  $G_{\rm eff}(t)$  may be computed as in a recent experimental study that quantifies polymer rheology using a rotational generalized Stokes-Einstein relation. 50 In this paper, we focus on reporting the scaling relations for the diffusion coefficients of nanorod, while leaving a detailed examination of  $\eta_{\text{eff}}$  and  $G_{\text{eff}}(t)$  for future research.

#### 4. CONCLUSIONS

To summarize, MD simulations of monomerically thin nanorods in polymer melts show a length-scale dependent coupling of nanorod diffusion and the polymer matrix, which is not resolved in current continuum theories.  $D_{\parallel} \sim l^{-1}$  if the melt chains are sufficiently long to screen the hydrodynamic interactions among different sections of a nanorod. In unentangled polymers, there is a crossover from  $D_{\perp} \sim l^{-2}$  to  $\sim l^{-1}$  with increasing l, as the rod is progressively coupled to larger segments of the polymer chains with partially screened hydrodynamic interactions. The diffusion anisotropy  $\kappa$ 

increases with l linearly and eventually saturates for sufficiently large l. The rotational diffusion coefficient  $D_{\rm R} \approx D_{\perp} l^{-2}$  and exhibits a crossover from  $D_{\rm R} \sim l^{-4}$  to  $\sim l^{-3}$ . In entangled polymers, the confinement by the entanglement network results in  $D_{\perp} \sim l^{-3}$  with  $\kappa \sim l^2$  and  $D_{\rm R} \sim l^{-5}$  for the nanorods with l sufficiently above a. The suppressed dependence of  $D_{\perp}$  and  $D_{\rm R}$  on l agrees with de Gennes' rod reptation model. <sup>53</sup>

For the diffusion of rodlike particles in Newtonian fluids, numerical expressions for diffusion coefficients have been obtained.  $^{28,61-66}$  It remains challenging to derive diffusion coefficients numerically for nanorods in polymer melts. The scaling relations we identify can serve as a foundation for the future development of new theories.  $^{67,68}$  With the absence of an analytical theory, they can also guide the experiments  $^{69-74}$  characterizing the transport of anisotropic nanoparticles in polymer matrices. Although  $D_{\rm T}$  is the most experimentally tractable diffusion coefficient,  $^{69,71}$  we hope that experimentalists would be motivated by this work to study  $D_{\parallel}$ ,  $D_{\perp}$ , and  $D_{\rm R}$ .

Our findings can provide insights into rodlike nano-objects diffusing in both synthetic gels<sup>75</sup> and their biological counterparts. The microscopic picture established here can also benefit the preparation of carbon nanotube—polymer composites, green polymer nanocomposites based on rodlike cellulose nanocrystals, and the understanding of how rodlike virus nanoparticles such as the tobacco mosaic virus transport in polymer solutions.

### ASSOCIATED CONTENT

### **5** Supporting Information

The Supporting Information is available free of charge at https://pubs.acs.org/doi/10.1021/acs.macromol.1c00989.

Parameters for simulation systems,  $R_g$  of nanorods, MSD and MSAD of nanorods, fitting results, and melt viscosity (PDF)

### AUTHOR INFORMATION

#### **Corresponding Author**

Ting Ge — Department of Chemistry and Biochemistry, University of South Carolina, Columbia, South Carolina 29208, United States; ⊙ orcid.org/0000-0003-2456-732X; Email: tingg@mailbox.sc.edu

### Authors

Jiuling Wang — Department of Chemistry and Biochemistry, University of South Carolina, Columbia, South Carolina 29208, United States; orcid.org/0000-0002-7379-3561

Thomas C. O'Connor — Sandia National Laboratories, Albuquerque, New Mexico 87185, United States;
occid.org/0000-0002-9393-0295

Gary S. Grest — Sandia National Laboratories, Albuquerque, New Mexico 87185, United States; ⊚ orcid.org/0000-0002-5260-9788

Yitong Zheng — Hongyi Honor School, Wuhan University, Wuhan, Hubei 430072, China; Department of Physics, School of Physics and Technology, Wuhan University, Wuhan, Hubei 430072, China

Michael Rubinstein — Thomas Lord Department of Mechanical Engineering and Materials Science, Departments of Biomedical Engineering, Chemistry, and Physics, Duke University, Durham, North Carolina 27708, United States; orcid.org/0000-0002-5455-0951

Complete contact information is available at: https://pubs.acs.org/10.1021/acs.macromol.1c00989

#### Notes

The authors declare no competing financial interest.

#### ACKNOWLEDGMENTS

The authors thank Christian Aponte-Rivera for stimulating discussion and comments on the manuscript. T.G. acknowledges start-up funds from the University of South Carolina. This work was supported in part by the National Science Foundation EPSCoR Program under NSF Award no. OIA-1655740. Any opinions, findings, and conclusions or recommendations expressed in this material are those of the authors and do not necessarily reflect those of the National Science Foundation. Y.Z. is grateful to the Visiting International Student Program funded by Duke University and Wuhan University. M.R. acknowledges the financial support from the National Science Foundation under grant EFMA-1830957 and the National Institutes of Health under grant P01-HL108808. Computational resources were provided by the University of South Carolina flagship computing cluster Hyperion. This research used resources at the National Energy Research Scientific Computing Center (NERSC), a U.S. Department of Energy Office of Science User Facility operated under Contract no. DE-AC02-05CH11231, and at the Oak Ridge Leadership Computing Facility at the Oak Ridge National Laboratory, which is supported by the Office of Science of the U.S. Department of Energy under Contract no. DE-AC05-00OR22725. These resources were obtained through the Advanced Scientific Computing Research (ASCR) Leadership Computing Challenge (ALCC). This work was performed, in part, at the Center for Integrated Nanotechnologies, an Office of Science User Facility operated for the U.S. Department of Energy (DOE) Office of Science. Sandia National Laboratories is a multimission laboratory managed and operated by the National Technology & Engineering Solutions of Sandia, LLC, a wholly owned subsidiary of Honeywell International, Inc., for the U.S. DOEs National Nuclear Security Administration under Contract no. DE-NA-0003525. The views expressed in the paper do not necessarily represent the views of the U.S. DOE or the United States Government.

### REFERENCES

- (1) Moniruzzaman, M.; Winey, K. I. Polymer nanocomposites containing carbon nanotubes. *Macromolecules* **2006**, *39*, 5194–5205.
- (2) Koerner, H.; Kelley, J.; George, J.; Drummy, L.; Mirau, P.; Bell, N. S.; Hsu, J. W.; Vaia, R. A. ZnO nanorod-thermoplastic polyurethane nanocomposites: morphology and shape memory performance. *Macromolecules* **2009**, *42*, 8933–8942.
- (3) McCook, N.; Boesl, B.; Burris, D.; Sawyer, W. Epoxy, ZnO, and PTFE nanocomposite: friction and wear optimization. *Tribol. Lett.* **2006**, 22, 253–257.
- (4) Brioude, A.; Jiang, X.; Pileni, M. Optical properties of gold nanorods: DDA simulations supported by experiments. *J. Phys. Chem. B* **2005**, *109*, 13138–13142.
- (5) Jain, P. K.; Eustis, S.; El-Sayed, M. A. Plasmon coupling in nanorod assemblies: optical absorption, discrete dipole approximation simulation, and exciton-coupling model. *J. Phys. Chem. B* **2006**, *110*, 18243–18253.
- (6) Hore, M. J.; Frischknecht, A. L.; Composto, R. J. Nanorod assemblies in polymer films and their dispersion-dependent optical properties. *ACS Macro Lett.* **2012**, *1*, 115–121.

- (7) Huynh, W. U.; Dittmer, J. J.; Alivisatos, A. P. Hybrid nanorod-polymer solar cells. *Science* **2002**, 295, 2425–2427.
- (8) White, S. I.; DiDonna, B. A.; Mu, M.; Lubensky, T. C.; Winey, K. I. Simulations and electrical conductivity of percolated networks of finite rods with various degrees of axial alignment. *Phys. Rev. B* **2009**, 79. No. 024301
- (9) White, S. I.; Mutiso, R. M.; Vora, P. M.; Jahnke, D.; Hsu, S.; Kikkawa, J. M.; Li, J.; Fischer, J. E.; Winey, K. I. Electrical percolation behavior in silver nanowire-polystyrene composites: simulation and experiment. *Adv. Funct. Mater.* **2010**, *20*, 2709–2716.
- (10) Mutiso, R. M.; Sherrott, M. C.; Li, J.; Winey, K. I. Simulations and generalized model of the effect of filler size dispersity on electrical percolation in rod networks. *Phys. Rev. B* **2012**, *86*, No. 214306.
- (11) Mutiso, R. M.; Sherrott, M. C.; Rathmell, A. R.; Wiley, B. J.; Winey, K. I. Integrating simulations and experiments to predict sheet resistance and optical transmittance in nanowire films for transparent conductors. *ACS Nano* **2013**, *7*, 7654–7663.
- (12) Hore, M. J.; Composto, R. J. Strategies for dispersing, assembling, and orienting nanorods in polymers. *Curr. Opin. Chem. Eng.* **2013**, *2*, 95–102.
- (13) Balazs, A. C.; Emrick, T.; Russell, T. P. Nanoparticle polymer composites: where two small worlds meet. *Science* **2006**, *314*, 1107–1110.
- (14) Jancar, J.; Douglas, J.; Starr, F. W.; Kumar, S.; Cassagnau, P.; Lesser, A.; Sternstein, S. S.; Buehler, M. Current issues in research on structure-property relationships in polymer nanocomposites. *Polymer* **2010**, *51*, 3321–3343.
- (15) Kumar, S. K.; Jouault, N.; Benicewicz, B.; Neely, T. Nanocomposites with polymer grafted nanoparticles. *Macromolecules* **2013**, *46*, 3199–3214.
- (16) Sankar, U. K.; Tripathy, M. Dispersion, depletion, and bridging of athermal and attractive nanorods in polymer melt. *Macromolecules* **2015**, *48*, 432–442.
- (17) Lu, S.; Wu, Z.; Jayaraman, A. Molecular Modeling and Simulation of Polymer Nanocomposites with Nanorod Fillers. *J. Phys. Chem. B* **2021**, *125*, 2435–2449.
- (18) Erigi, U.; Dhumal, U.; Tripathy, M. Phase behavior of polymernanorod composites: A comparative study using PRISM theory and molecular dynamics simulations. *J. Chem. Phys.* **2021**, *154*, No. 124903.
- (19) Alam, S.; Mukhopadhyay, A. Translational and rotational diffusions of nanorods within semidilute and entangled polymer solutions. *Macromolecules* **2014**, *47*, 6919–6924.
- (20) Choi, J.; Cargnello, M.; Murray, C. B.; Clarke, N.; Winey, K. I.; Composto, R. J. Fast nanorod diffusion through entangled polymer melts. *ACS Macro Lett.* **2015**, *4*, 952–956.
- (21) Karatrantos, A.; Composto, R. J.; Winey, K. I.; Clarke, N. Nanorod diffusion in polymer nanocomposites by molecular dynamics simulations. *Macromolecules* **2019**, *52*, 2513–2520.
- (22) Yu, M.; Wang, J.; Yang, Y.; Zhu, C.; Su, Q.; Guo, S.; Sun, J.; Gan, Y.; Shi, X.; Gao, H. Rotation-facilitated rapid transport of nanorods in mucosal tissues. *Nano Lett.* **2016**, *16*, 7176–7182.
- (23) Bao, C.; Liu, B.; Li, B.; Chai, J.; Zhang, L.; Jiao, L.; Li, D.; Yu, Z.; Ren, F.; Shi, X.; Li, Y. Enhanced Transport of Shape and Rigidity-tuned  $\alpha$ -lactalbumin Nanotubes across Intestinal Mucus and Cellular Barriers. *Nano Lett.* **2020**, *20*, 1352–1361.
- (24) Bao, W.; Tian, F.; Lyu, C.; Liu, B.; Li, B.; Zhang, L.; Liu, X.; Li, F.; Li, D.; Gao, X.; et al. Experimental and theoretical explorations of nanocarriers' multistep delivery performance for rational design and anticancer prediction. *Sci. Adv.* **2021**, *7*, No. eaba2458.
- (25) Wang, J.; Yang, Y.; Yu, M.; Hu, G.; Gan, Y.; Gao, H.; Shi, X. Diffusion of rod-like nanoparticles in non-adhesive and adhesive porous polymeric gels. *J. Mech. Phys. Solids* **2018**, *112*, 431–457.
- (26) Wang, J.; Shi, X. Molecular dynamics simulation of diffusion of nanoparticles in mucus. *Acta Mech. Solida Sin.* **2017**, *30*, 241–247.
- (27) Doi, M.; Edwards, S. F. The Theory of Polymer Dynamics; Oxford University Press, 1988.

- (28) Happel, J.; Brenner, H. Low Reynolds Number Hydrodynamics: With Special Applications to Particulate Media; Martinus Nijhoff: The Hague, 1983.
- (29) Li, S.-J.; Qian, H.-J.; Lu, Z.-Y. Translational and rotational dynamics of an ultra-thin nanorod probe particle in linear polymer melts. *Phys. Chem. Chem. Phys.* **2018**, *20*, 20996–21007.
- (30) Tuteja, A.; Mackay, M. E.; Narayanan, S.; Asokan, S.; Wong, M. S. Breakdown of the continuum Stokes-Einstein relation for nanoparticle diffusion. *Nano Lett.* **2007**, *7*, 1276–1281.
- (31) Cai, L.-H.; Panyukov, S.; Rubinstein, M. Mobility of nonsticky nanoparticles in polymer liquids. *Macromolecules* **2011**, *44*, 7853–7863.
- (32) Yamamoto, U.; Schweizer, K. S. Theory of nanoparticle diffusion in unentangled and entangled polymer melts. *J. Chem. Phys.* **2011**, *135*, No. 224902.
- (33) Kalathi, J. T.; Yamamoto, U.; Schweizer, K. S.; Grest, G. S.; Kumar, S. K. Nanoparticle diffusion in polymer nanocomposites. *Phys. Rev. Lett.* **2014**, *112*, No. 108301.
- (34) Yamamoto, U.; Schweizer, K. S. Microscopic theory of the long-time diffusivity and intermediate-time anomalous transport of a nanoparticle in polymer melts. *Macromolecules* **2015**, *48*, 152–163.
- (35) Ge, T.; Grest, G. S.; Rubinstein, M. Nanorheology of entangled polymer melts. *Phys. Rev. Lett.* **2018**, *120*, No. 057801.
- (36) Xue, C.; Zheng, X.; Chen, K.; Tian, Y.; Hu, G. Probing non-Gaussianity in confined diffusion of nanoparticles. *J. Phys. Chem. Lett.* **2016**, *7*, 514–519.
- (37) Xue, C.; Shi, X.; Tian, Y.; Zheng, X.; Hu, G. Diffusion of Nanoparticles with Activated Hopping in Crowded Polymer Solutions. *Nano Lett.* **2020**, 20, 3895–3904.
- (38) Han, Y.; Alsayed, A. M.; Nobili, M.; Zhang, J.; Lubensky, T. C.; Yodh, A. G. Brownian motion of an ellipsoid. *Science* **2006**, *314*, 626–630.
- (39) Kremer, K.; Grest, G. S. Dynamics of entangled linear polymer melts: A molecular dynamics simulation. *J. Chem. Phys.* **1990**, *92*, 5057–5086.
- (40) Grest, G. S. Communication: Polymer entanglement dynamics: Role of attractive interactions. *J. Chem. Phys.* **2016**, *145*, No. 141101.
- (41) Hsu, H.-P.; Kremer, K. Static and dynamic properties of large polymer melts in equilibrium. *J. Chem. Phys.* **2016**, *144*, No. 154907.
- (42) Everaers, R.; Karimi-Varzaneh, H. A.; Fleck, F.; Hojdis, N.; Svaneborg, C. Kremer-Grest Models for Commodity Polymer Melts: Linking Theory, Experiment, and Simulation at the Kuhn Scale. *Macromolecules* **2020**, 53, 1901–1916.
- (43) Plimpton, S. Fast parallel algorithms for short-range molecular dynamics. *J. Comput. Phys.* **1995**, *117*, 1–19.
- (44) Lobaskin, V.; Dünweg, B. A new model for simulating colloidal dynamics. *New J. Phys.* **2004**, *6*, No. 54.
- (45) Yeh, I.-C.; Hummer, G. System-size dependence of diffusion coefficients and viscosities from molecular dynamics simulations with periodic boundary conditions. *J. Phys. Chem. B* **2004**, *108*, 15873–15879
- (46) Li, Z. Critical particle size where the Stokes-Einstein relation breaks down. *Phys. Rev. E* **2009**, *80*, No. 061204.
- (47) More precisely, one should distinguish  $\zeta_0^{\parallel}$  experienced by the beads at the two ends of the rod and  $\zeta_0^{\parallel}$  for the non-end beads.
- (48) Brochard Wyart, F.; de Gennes, P.-G. Viscosity at small scales in polymer melts. *Eur. Phys. J. E: Soft Matter* **2000**, *1*, 93–97.
- (49) Aponte-Rivera, C. Private communication.
- (50) Molaei, M.; Atefi, E.; Crocker, J. C. Nanoscale rheology and anisotropic diffusion using single gold nanorod probes. *Phys. Rev. Lett.* **2018**, *120*, No. 118002.
- (51) A numerical determination of  $\tau_{\rm T}$  from  $\langle \Delta r_{\perp}^2(t) \rangle / 4t$  requires a theoretical description that resolves the time-dependent feature of the nanorod motion.
- (52) Everaers, R.; Sukumaran, S. K.; Grest, G. S.; Svaneborg, C.; Sivasubramanian, A.; Kremer, K. Rheology and microscopic topology of entangled polymeric liquids. *Science* **2004**, *303*, 823–826.
- (53) de Gennes, P. G. Motions of one stiff molecule in an entangled polymer melt. *J. Phys. France* **1981**, *42*, 473–477.

- (54) Cai, L.-H.; Panyukov, S.; Rubinstein, M. Hopping diffusion of nanoparticles in polymer matrices. *Macromolecules* **2015**, *48*, 847–862
- (55) Ge, T.; Kalathi, J. T.; Halverson, J. D.; Grest, G. S.; Rubinstein, M. Nanoparticle motion in entangled melts of linear and non-concatenated ring polymers. *Macromolecules* **2017**, *50*, 1749–1754.
- (56) Squires, T. M.; Mason, T. G. Fluid mechanics of microrheology. Annu. Rev. Fluid Mech. 2010, 42, 413-438.
- (57) Indei, T.; Schieber, J. D.; Córdoba, A.; Pilyugina, E. Treating inertia in passive microbead rheology. *Phys. Rev. E* **2012**, 85, No. 021504
- (58) Karim, M.; Kohale, S. C.; Indei, T.; Schieber, J. D.; Khare, R. Determination of viscoelastic properties by analysis of probe-particle motion in molecular simulations. *Phys. Rev. E* **2012**, *86*, No. 051501.
- (59) Karim, M.; Indei, T.; Schieber, J. D.; Khare, R. Determination of linear viscoelastic properties of an entangled polymer melt by probe rheology simulations. *Phys. Rev. E* **2016**, *93*, No. 012501.
- (60) Aponte-Rivera, C.; Rubinstein, M. Dynamic coupling in unentangled liquid coacervates formed by oppositely charged polyelectrolytes. *Macromolecules* **2021**, *54*, 1783–1800.
- (61) Tirado, M. M.; de la Torre, J. G. Translational friction coefficients of rigid, symmetric top macromolecules. Application to circular cylinders. *J. Chem. Phys.* **1979**, *71*, 2581–2587.
- (62) Tirado, M. M.; de la Torre, J. G. Rotational dynamics of rigid, symmetric top macromolecules. Application to circular cylinders. *J. Chem. Phys.* **1980**, 73, 1986–1993.
- (63) Tirado, M. M.; Martínez, C. L.; de la Torre, J. G. Comparison of theories for the translational and rotational diffusion coefficients of rod-like macromolecules. Application to short DNA fragments. *J. Chem. Phys.* **1984**, *81*, 2047–2052.
- (64) Broersma, S. Rotational diffusion constant of a cylindrical particle. *J. Chem. Phys.* **1960**, *32*, 1626–1631.
- (65) Broersma, S. Viscous force constant for a closed cylinder. J. Chem. Phys. 1960, 32, 1632–1635.
- (66) Brenner, H. Rheology of a dilute suspension of axisymmetric Brownian particles. *Int. J. Multiphase Flow* **1974**, *1*, 195–341.
- (67) Yamamoto, U.; Schweizer, K. S. Theory of entanglements and tube confinement in rod-sphere nanocomposites. *ACS Macro Lett.* **2013**, *2*, 955–959.
- (68) Yamamoto, U.; Schweizer, K. S. Theory of anisotropic diffusion of entangled and unentangled polymers in rod-sphere mixtures. *ACS Macro Lett.* **2015**, *4*, 53–57.
- (69) Bailey, E. J.; Winey, K. I. Dynamics of polymer segments, polymer chains, and nanoparticles in polymer nanocomposite melts: A review. *Prog. Polym. Sci.* **2020**, *105*, No. 101242.
- (70) Park, J.; Bailey, E. J.; Composto, R. J.; Winey, K. I. Single-particle tracking of nonsticky and sticky nanoparticles in polymer melts. *Macromolecules* **2020**, *53*, 3933–3939.
- (71) Rose, K. A.; Molaei, M.; Boyle, M. J.; Lee, D.; Crocker, J. C.; Composto, R. J. Particle tracking of nanoparticles in soft matter. *J. Appl. Phys.* **2020**, *127*, No. 191101.
- (72) Gratz, M.; Tschöpe, A. Size effects in the oscillatory rotation dynamics of Ni nanorods in poly (ethylene oxide) solutions. *Macromolecules* **2019**, *52*, 6600–6612.
- (73) Hess, M.; Gratz, M.; Remmer, H.; Webers, S.; Landers, J.; Borin, D.; Ludwig, F.; Wende, H.; Odenbach, S.; Tschöpe, A.; Schmidt, A. M. Scale-dependent particle diffusivity and apparent viscosity in polymer solutions as probed by dynamic magnetic nanorheology. *Soft Matter* **2020**, *16*, 7562–7575.
- (74) Lee, J.; Grein-Iankovski, A.; Narayanan, S.; Leheny, R. L. Nanorod mobility within entangled wormlike micelle solutions. *Macromolecules* **2017**, *50*, 406–415.
- (75) Fakhri, N.; MacKintosh, F. C.; Lounis, B.; Cognet, L.; Pasquali, M. Brownian motion of stiff filaments in a crowded environment. *Science* **2010**, 330, 1804–1807.
- (76) Papageorgiou, D. G.; Li, Z.; Liu, M.; Kinloch, I. A.; Young, R. J. Mechanisms of mechanical reinforcement by graphene and carbon nanotubes in polymer nanocomposites. *Nanoscale* **2020**, *12*, 2228–2267.

- (77) Song, L.; Wang, Z.; Lamm, M. E.; Yuan, L.; Tang, C. Supramolecular polymer nanocomposites derived from plant oils and cellulose nanocrystals. *Macromolecules* **2017**, *50*, 7475–7483.
- (78) Cush, R.; Dorman, D.; Russo, P. S. Rotational and Translational Diffusion of Tobacco Mosaic Virus in Extended and Globular Polymer Solutions. *Macromolecules* **2004**, *37*, 9577–9584.
- (79) Smith, M.; Poling-Skutvik, R.; Slim, A. H.; Willson, R. C.; Conrad, J. C. Dynamics of Flexible Viruses in Polymer Solutions. *Macromolecules* **2021**, *54*, 4557–4563.